COMPATIBILITY ASSESSMENT OF NON-STEEL METALLIC DISTRIBUTION GAS GRID MATERIALS WITH HYDROGEN


# D2.3

# Literature review on hydrogen embrittlement of cast iron and non-ferrous alloys


| | |
|---|---|
| **Marina Cabrini *** | UNIBG |
| Denny Coffetti | UNIBG |

***Corresponding author**



Clean Hydrogen Partnership

*The project is supported by the Clean Hydrogen Partnership and its members.*

Co-funded by the European Union

# TECHNICAL REFERENCES

| | |
|---|---|
| **Project Acronym** | CANDHy |
| **Project Title** | COMPATIBILITY ASSESSMENT OF NON-STEEL METALLIC DISTRIBUTION GAS GRID MATERIALS WITH HYDROGEN |
| **Type** | Report |
| **Call Identifier** | HORIZON-JTI-CLEANH2-2022-02-01 |
| **Topic** | Compatibility of Distribution non-steel metallic gas grid materials with hydrogen |
| **Project Coordinator** | Fundación para el Desarrollo de las Nuevas Tecnologías del Hidrógeno en Aragón (FHa) |
| **Project Duration** | 36 months |

| | |
|---|---|
| **Deliverable No.** | D 2.4 |
| **Dissemination Level** | PU-Public |
| **Work Package** | WP2 - Review of the state of the art of the grid material and existing standards |
| **Task** | T 2.4 – Literature review on hydrogen embrittlement of cast iron and non-ferrous alloys |
| **Lead beneficiary** | 8 (UNIBG) |
| **Contributing beneficiary** | 1 (FHa) |
| **Due date of deliverable** | 30/10/24 |
| **Actual submission date** | 08/11/24 |

# VERSIONS

| Revision Version | Date | Changes | Changes made by Partner |
|---|---|---|---|
| 0.1 | 18 October 2024 | First release | M. Cabrini (UNIBG)<br>D. Coffetti (UNIBG) |
| 0.2 | 25 October 2024 | Revision | M.Cabrini (UNIBG)<br>D.Coffetti (UNIBG)<br>E.Soileux (RINA) |
| 1.0 | 04 November 2024 | Revision | Matías Suárez (FHa)<br>Vanesa Gil (ARAID/FHa) |
| 1.1 | 05 November 2024 | Final revision | M. Cabrini (UNIBG) |
| 2.0 | 08 November 2024 | Final document | Lidia Martínez (FHa) |

Co-funded by the European Union. Views and opinions expressed are however those of the author(s) only and do not necessarily reflect those of the European Union or the Clean Hydrogen Partnership. Neither the European Union nor the granting authority can be held responsible for them.

# Table of Content

# EXECUTIVE SUMMARY

The intention of the European gas industry is to enable the use of natural gas infrastructure for hydrogen. However, for the use of hydrogen in the natural gas infrastructure the consequences or the impact of hydrogen on the gas system need to be identified. Carbon steel is the alloy family of metallic materials most used in hydrogen gas distribution pipelines and is suitability in hydrogen gas is well studied and reported. On the contrary, studies on non-steel metallic materials also present in the current gas grid distribution networks are limited and the effect of hydrogen embrittlement (HE) on these materials needs to be comprehensible understood.

As gas distribution networks operate at low pressure, < 16 bar, these networks are less standardized than transport networks. CANDHy project focuses on the compatibility assessment of non-steel metallic distribution gas grid materials with hydrogen in European countries.

As part of Task 2.4 of CANDHy Work Package 2 (WP2) a full review of the hydrogen dissociation, solubility and diffusion in non-steel metallic materials was performed.

In this document, gaseous hydrogen dissociation and adsorption on metals, electrochemical hydrogen evolution and hydrogen diffusion are briefly described, with the main mechanism of hydrogen embrittlement. The work focuses on hydrogen diffusion and embrittlement on cast iron, copper and lead.

Existing literature generally suggests that these materials exhibit no significant effects when exposed to high-pressure gaseous hydrogen at room temperature. However, some detrimental effects can be observed during hydrogen electrochemical charging or exposure to high-temperature $H_2$ environments. Hydrogen embrittlement (HE) effects were observed on cast iron under cathodic polarization. HE effects were related to size and distribution of graphite inside the alloy, owing to their traps effect for hydrogen. The solubility of hydrogen in copper and its alloys is very low at room temperature thus no detrimental effects were observed. Hydrogen molecule dissociation does not take place on lead at room temperature. If lead is polarized with very high cathodic current density in alkaline solution, lead can degrade through the formation of a volatile lead hydride.

# 1. INTRODUCTION AND OBJECTIVES

The transportation of gaseous hydrogen through metallic pipelines has been occurring globally for over 80 years. By 2012, approximately 3,200 kilometers of hydrogen transmission pipelines were operating at pressures up to 10 MPa [1]. Some design codes and standards for hydrogen transport and storage equipment are documented in [1].

Numerous studies have explored the viability of blending hydrogen into natural gas pipelines made of carbon steel. However, there is limited understanding of how hydrogen affects other metallic materials present in the natural gas distribution network, such as cast iron, copper alloys, and lead.

Understanding the impact of hydrogen on these materials is crucial for the successful development and implementation of green hydrogen and the ecological transition. This report detailed the work performed for CANDHY Work Package 2 Task 2.4. UNIBG was the task leader.

This review examines hydrogen dissociation, diffusion, and embrittlement in various metallic materials. Additionally, it focuses on hydrogen diffusion and its effects on cast iron, copper, and lead materials.

## 2. HYDROGEN EMBRITTLEMENT

Hydrogen embrittlement (HE) is a specific type of Environmental Assisted Cracking (EAC). The term EAC refers to the phenomenon caused by the synergistic interaction between a susceptible material, a particular environment, and tensile stress (Figure 1). This process leads to crack formation, which propagates due to the combined effect of stress and environmental factors, potentially resulting in the failure of structural components, even under loads significantly below the material's tensile strength. For HE to occur, atomic hydrogen must be present within a susceptible metal under mechanical stress.

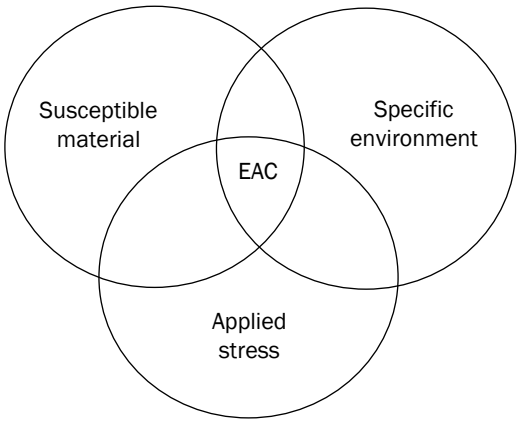


Figure 1. Schematic representation of EAC phenomena

## 3. ATOMIC HYDROGEN ADSORPTION AND ABSORPTION

Atomic hydrogen has considerable solubility and relatively high diffusion rates in metallic lattices, even at room temperature, due to its small atomic size. Hydrogen can be present in molten metal or incorporated during welding, but more commonly, it enters steel through atomic adsorption on the metal's surface when in contact with an external environment.

### 3.1 Hydrogen adsorption by electrochemical reduction of $H^+$ or $H_2O$

Hydrogen can be generated by the electrochemical reduction of water or $H^+$ ions during corrosion or cathodic polarization (CP). When a cathodic potential lower than the thermodynamic threshold for hydrogen evolution is applied, hydrogen evolves on the steel surface. The reduction of hydrogen ions in neutral solutions occurs according to the following mechanism:

$$(1) \qquad H_2O_{sol} + e^-_{met} \rightarrow H^{\cdot}_{ads,met}$$

$$(2) \qquad H^{\cdot}_{ads,met} + H_2O_{sol} + e^-_{met} \rightarrow H_2$$

$$(3) \qquad H^{\cdot}_{ads,met} + H^{\cdot}_{ads,met} \rightarrow H_2$$

Some of the adsorbed hydrogen on the surface of the metal ($H_{ads}$) diffuses into the metal lattice and is absorbed ($H_{abs}$):

$$(4) \qquad H^{\cdot}_{ads,met} \rightarrow H^{\cdot}_{abs}$$

## 3.2 Hydrogen adsorption by dissociation of $H_2$ molecules

Hydrogen can be adsorbed either as a molecule (physisorption) or as an atom (dissociative chemisorption). Adsorption occurs at the gas-solid interface within a nanometer-thick region [2] . Figure 2 illustrates the energetic interaction between hydrogen and the metal surface. When hydrogen approaches the surface, weak van der Waals forces cause the $H_2$ molecule to move into a shallow potential energy well with $E_p$ located at the distance $z_p$ from the surface. If hydrogen is forced closer, strong repulsive forces arise.

The equilibrium position of physically adsorbed hydrogen is represented by $z_p$, and the corresponding energy ($E_p$) is relatively low, typically just a few kJ/mol. This makes physical adsorption achievable only at sufficiently low temperatures when the molecule's thermal energy is low [3]. In cases where hydrogen's molecular orbitals interact with the metal's Fermi level, tunneling occurs and electrons populate antibonding orbitals. This leads to the weakening of the H-H bonds, causing the molecular orbitals to shift below the Fermi level, and the molecule dissociates. The dissociated atoms form bonds with the surface, leading to chemisorption. The electrons of the two dissociated hydrogen atoms independently interact with the substrate establishing chemical bonds with the surface [2].

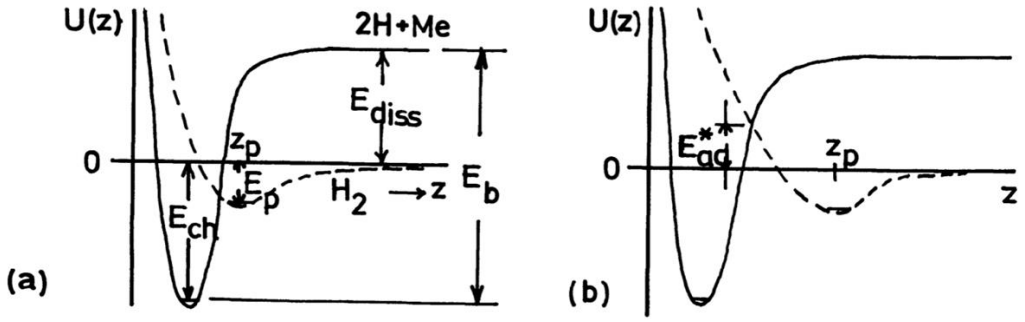


Figure 2. Potential energy diagram for hydrogen adsorption according to Lennard-Jones. Example (a) refers to non-activated adsorption with the point of intersection of the two potential curves below E = 0, example (b) illustrates the case of activated adsorption with the intersection above E =0 [3]

The chemi-adsorption process of the $H_2$ molecule can be summarize with the reversible reaction [4]:

$$(5) \qquad H_2 + 2M \rightleftarrows 2H_{ad} + 2M \rightleftarrows 2MH$$

The energy required to dissociate an $H_2$ molecule into atoms is 432 kJ/mol [3]. The ability of different metals to facilitate this dissociation varies depending on their intrinsic properties [5].

$H_2$ can dissociate via two distinct pathways (Figure 3): (i) homolytic dissociation, where the metal center bonds to another metal atom within its coordination sphere to form a metal–metal pair; and (ii) heterolytic dissociation, where the metal center bonds to a Lewis base to form a metal–base pair (base = O, S, N, P) [6].

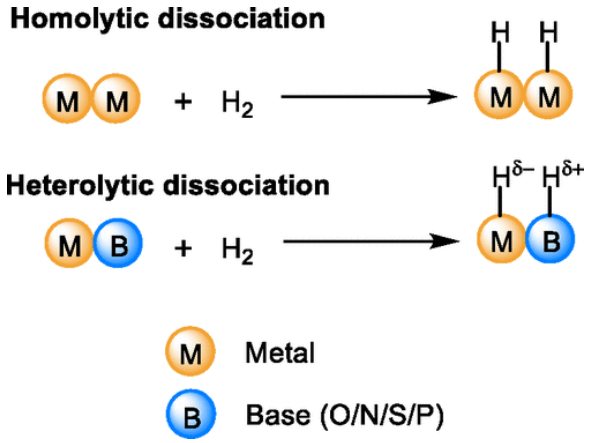


Figure 3. Illustration of $H_2$ dissociation pathways [6]

On clean metal surfaces, hydrogen typically dissociates via the homolytic pathway. The nature of the resulting M–H bond depends on the metal's electronegativity: metals with lower electronegativity, such as alkali and alkaline earth metals, tend to form hydridic ($M–H^{\delta-}$) bonds, while late transition metals, with electronegativities like that of hydrogen, form predominantly covalent M–H bonds. Heterolytic dissociation can occur if the local coordination structures of the metal centers satisfy the Lewis acid–base pair criterion (metal–base, base = O, S, N, P). Due to the structural heterogeneity of metal surfaces, metal–metal and metal–base sites coexist, allowing for both homolytic and heterolytic dissociation pathways to contribute to hydrogen dissociation. However, the heterolytic pathway is less likely to significantly affect overall reaction kinetics due to its relatively high energy barrier unless the homolysis sites (metal–metal pairs) are absent or blocked [6].

The bond energy for the M–H bond typically ranges between 500 and 600 kJ/mol, depending on the metal's chemical nature and the atomic density of the exposed surface (Figure 4). The chemisorption of $H_2$ on most late transition metals (except Au and Ag) is exothermic [6].

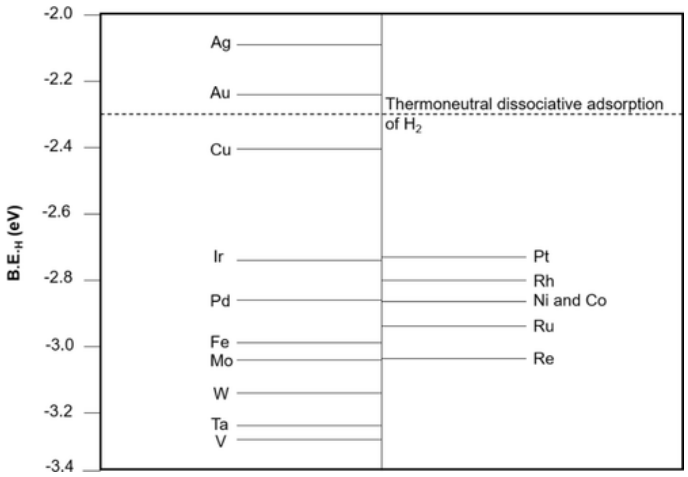


Figure 4. Binding energies of gas-phase atomic hydrogen (B.E.$_H$) on various close-packed clean metal surfaces. The dashed line denotes thermoneutral dissociative adsorption of $H_2$ [6]

The equilibrium position for chemisorbed hydrogen, given by the distance $z_{ch}$ in Figure 2, is much closer to the metal surface than the position $z_p$ for physically adsorbed hydrogen. Due to the considerable depth of the chemisorption energy well, hydrogen atoms will rarely escape from this state, even at room temperature [3].

Homolytic dissociation and adsorption of hydrogen can occur either with or without activation, depending on whether the crossover point between the physisorption and chemisorption potential energy curves lies above or below the zero potential energy line. Figure 2a illustrates a case where no activation barrier is present, allowing spontaneous dissociation of the hydrogen molecule. In contrast, Figure 2b shows a scenario where an additional activation energy $E^*_{ad}$ is required. For most transition metals, hydrogen adsorption is non-activated, and the chemisorption process occurs readily. However, in some cases, kinetic limitations may slow down the process significantly. For example, hydrogen adsorption on a Cu (111) surface is activated by approximately 12 kJ/mol. This means that only relatively high hydrogen pressures and elevated surface temperatures enable sufficient hydrogen molecules to overcome the activation barrier and undergo dissociation. Once dissociation occurs, the Cu–H chemisorption bond forms readily, with its bond strength aligning with the average $E_b$ values for other metals [3].

When multiple hydrogen atoms are adsorbed onto closed sites, repulsive or attractive forces may arise. As a result, the hydrogen-metal binding energy $E_b$ (and consequently the heat of adsorption $E_{ch}$) depends on the concentration and arrangement of the adsorbed hydrogen atoms. Typically, as coverage increases, $E_{ch}$ gradually decreases [3].

Hydrogen atoms may also penetrate through the first metal layer, settling in potential wells within the material, creating adsorption sites that are energetically intermediate between adsorption and absorption. Defects and impurities in the metal create a wide variety of adsorption sites. The sticking probability, heat of adsorption, and activation energy for desorption depend on the degree of coverage and they are highest when the surface has minimal coverage [2].

Surface impurities can dramatically alter hydrogen interaction with metal. Gaseous impurities may block dissociation sites, competing with hydrogen for adsorption locations. Even small concentrations of

impurities can be sufficient to block these sites, significantly reducing the rate of dissociative chemisorption. More active molecules like $O_2$ and CO often limit hydrogen uptake by occupying adsorption sites, thereby inhibiting hydrogen embrittlement [7]. As a result, hydrogen adsorption is most efficient on newly exposed, active surfaces, such as those subjected to mechanical straining during slow strain rate tests or fatigue crack propagation.

## 3.3 From adsorption to absorption

The penetration of hydrogen atoms through the surface may lead to their accommodation below the surface, a process often called "sub-surface adsorption." From this point, hydrogen atoms can diffuse into the metal lattice.

The absorption of half hydrogen gas molecules by a metal can be described by the reaction:

$$M + \frac{x}{2} H_2 \rightarrow MH_x + x\Delta H \quad (6)$$

where *ΔH* is the enthalpy of solution, representing the heat released per absorbed hydrogen atom. The value of *ΔH* is positive for exothermic absorption and negative for endothermic absorption. Various materials exhibit different enthalpies of solution (Figure 5) as reported in [8].

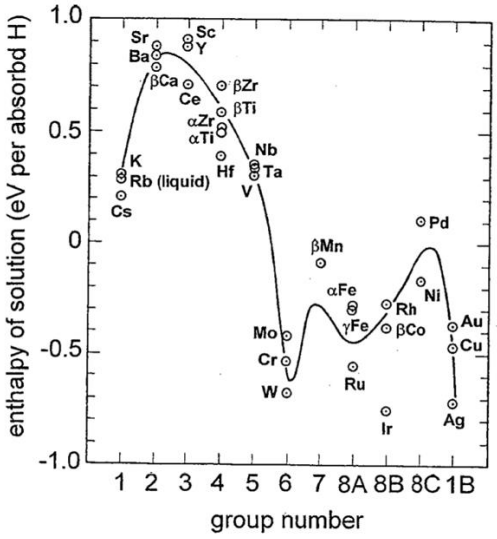


Figure 5. Enthalpy of solution ΔH for hydrogen absorption by various metals (the values hold in the limit of small hydrogen concentrations and for hydrogen gas pressures of hydrogen up to a hundred bar, for which the hydrogen gas can be assumed to be ideal [8]

For lattice diffusion-controlled transport, hydrogen gas is in thermodynamic equilibrium with sub-surface hydrogen. The solubility of hydrogen is expressed as the ratio of permeability to diffusivity. According to Sievert's law, the solubility of a bi-atomic gas inside a metal membrane is given by:

$$c_H = S \cdot \sqrt{p} + c_T \quad (7)$$

Where $c_T$ refers to trapped hydrogen, $S$ is the gas solubility, and $p$ is the external pressure [9]. The square root dependence on $p$ arises from the dissociation of the hydrogen molecule into two atoms, which distribute themselves over interstitial sites within the metal lattice [10].

At very high pressures, deviations from ideal gas behavior occur [11]. In such cases, pressure is replaced by fugacity ($f_{H2}$) which correlates with pressure as:

$$f_{H_2} = pe^{\frac{pb}{RT}} \quad (8)$$

Where $b$ is a constant, $T$ the temperature and $R$ the universal gas constant [12]. The relationship between pressure and fugacity for hydrogen is illustrated in Figure 6 [11].

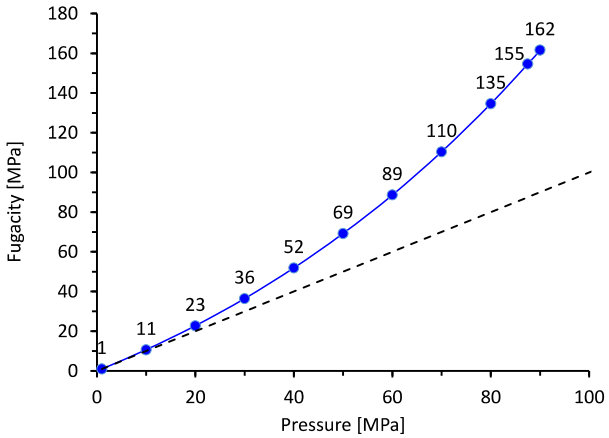


Figure 6. Correlation between pressure and fugacity of hydrogen evaluated at room temperature by [11]

When the pressure is reduced to a point where the active surface is no longer fully covered by hydrogen gas, the pressure dependence becomes linear. This behavior fits the Langmuir chemisorption model:

$$\theta = \frac{bp}{1+bp} \quad (9)$$

Where $\theta$ is fraction of surface covered by hydrogen, $p$ is the hydrogen pressure and $b$ a constant.

## 3.4 Adsorption hydrogen diffusion

The diffusion of hydrogen in steel has been widely studied. The hydrogen flux is proportional to the concentration gradient between the surface and the metal lattice. Several factors influence hydrogen solubility and diffusion, including the steel's microstructure, the presence of second phases, and mechanical stress.

According to Oriani's theory [13], hydrogen migrates through the interstitial sites of the metal's crystal lattice (normal interstitial lattice sites – NILS) or becomes trapped in microstructural defects like dislocations, grain boundaries, and carbides. In an ideally homogeneous lattice, the depth of potential wells and the activation energy between adjacent sites would be equal. However, various preferential

diffusion paths and traps with lower activation energy disrupt the process, slowing down hydrogen diffusion.

Traps are typically classified as either reversible or irreversible, based on their binding energy with hydrogen. Reversible traps release hydrogen at room temperature when surface concentrations decrease, while irreversible traps, with higher binding energies, can only release hydrogen at elevated temperatures [14].

Traps can also be identified as saturable, if they can retain only one hydrogen atom (or a finite number), or not saturable, if they can accommodate any quantity of hydrogen (i.e. blisters) [14] [15] [16] [17]. Hydrogen is typically irreversibly trapped at the interface between non-metallic inclusions and precipitates like MnS, $Al_2O_3$ and TiC [18] [19] [20] [21] [16], [22], [23] [24] [25].

In the absence of traps or preferential paths, the unsteady diffusion of hydrogen atoms in metals can be described using Fick's second law:

$$\frac{dC}{dt} = D\nabla^2 C \quad (10)$$

Where D is the diffusion coefficient through metal lattice.

When traps are present, this equation is modified by introducing an apparent diffusion coefficient $D_{app}^{H}$, accounting for the local equilibrium between mobile and trapped hydrogen populations [13]:

$$D_{app}^{H} = D_{\alpha}^{H} \cdot \left[1 + \frac{N^H}{N^L} e^{\left(\frac{E_b}{RT}\right)}\right]^{-1} \quad (11)$$

where $N_L$ is the number of normal sites per unit volume, $N_H$ is the number of trap sites per unit volume and $E_b$ is binding energy between the trap and hydrogen.

The steady-state flux of hydrogen permeating through a structure is given by Fick's first law of diffusion [26]:

$$J = -D\frac{dc}{dx} \quad (12)$$

This equation can be integrated between the thickness ($L$) of the metal and, assuming the hydrogen concentration at the exit side zero, the steady-state hydrogen flux becomes:

$$J_{\propto} = -D\frac{C_H}{L} \quad (13)$$

The value of $C^H$ can be obtained by means of the Sievert's law:

$$J_{\infty} = D\frac{S\sqrt{f}}{L} \quad (14)$$

Where $S$ is the hydrogen solubility in the steel and $f$ its fugacity.

Considering the permeability ($\Phi$) as the product of the hydrogen diffusion coefficient ($D$) for the solubility ($S$):

$$\Phi \equiv D \cdot S \quad (15)$$

the equation becomes:

$$(16) \quad J_\infty = \frac{\Phi\sqrt{f}}{L}$$

Were $J_\infty$ represents the steady state diffusional flux of hydrogen, $L$ is the structure thickness of the material and $f$ is the fugacity of hydrogen gas of the high pressure side of the plate.

For any metal, hydrogen solubility and its diffusion coefficient within the metal lattice are only temperature dependent. Therefore, at constant temperature, the hydrogen permeation flux depends solely on the hydrogen pressure (fugacity).

Figure 7 shows the linear correlation between hydrogen permeation flux and the logarithm of pressure for alpha iron, 1050 and 1055 steels. Although the temperature is unspecified, the tests were conducted in the range of 500 to 900 K [8]. Typically, hydrogen transport properties are measured at elevated temperature to simplify the process.

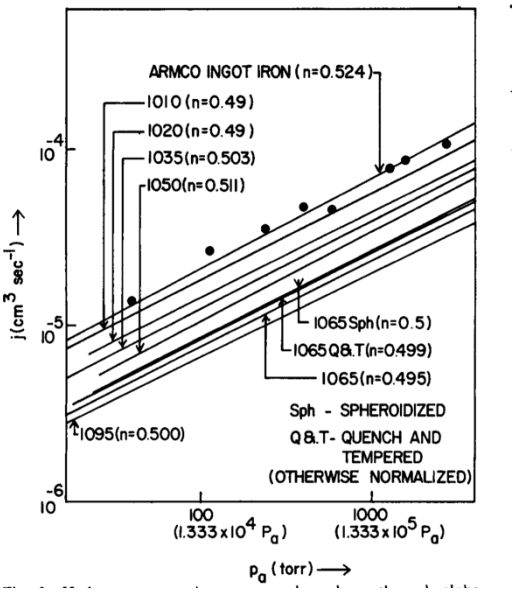


Figure 7. Hydrogen permeation pressure dependence through alpha iron, carbon steels and heat treated 1065 steel [27]

Data on gaseous hydrogen diffusion at low temperature is limited, but electrochemical methods can be used to obtain such data. San Marchi and Somerday noted that electrochemical permeation measurements (ASTM G148 - standardized in 2004 as ISO International Standard 17081) are not recommended for determining hydrogen transport properties in materials exposed to high-pressure hydrogen gas, though they can be used in the absence of gas permeation data [26]. Figure 8 provides data on X60/70 steel from Feng *et al.* [28].

Hydrogen diffusion in steel is primarily influenced by the microstructure, the presence of secondary phases, and mechanical stress.

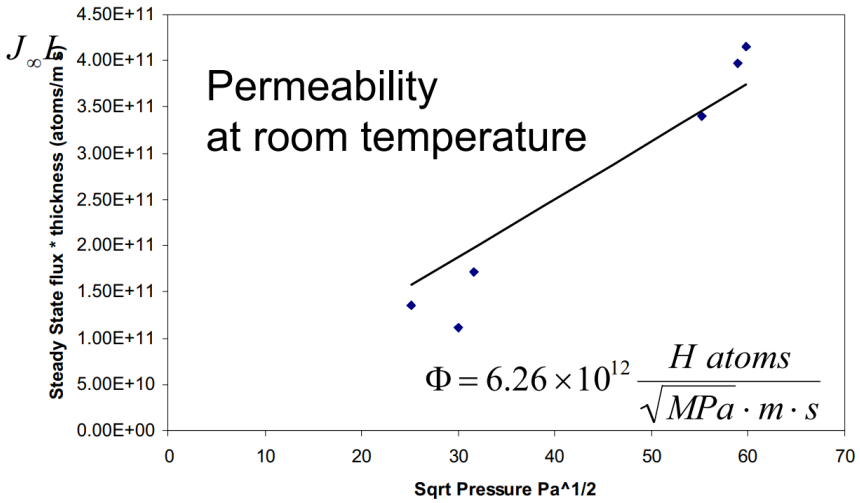


Figure 8. Relationship between hydrogen steady state flux and pressure at room temperature [28]

## 4. HYDROGEN EMBRITTLEMENT

Atomic hydrogen can diffuse through metals and migrate to areas of high stress concentration, leading to failures [29] [30]. Hydrogen embrittlement (HE) was first documented by Johnson in 1875, where he reported a reduction in the ductility and fracture strength of iron due to hydrogen exposure [31] [32]. Zielinski and Domzalicki [33] observed a strong linear correlation between hydrogen degradation (measured as loss of mechanical properties or reduced time-to-failure) and the content of diffusible hydrogen in high-strength steels. However, there was no such correlation with total hydrogen content. They concluded that susceptibility to hydrogen embrittlement in high-strength low-alloy steels depends primarily on the amount of mobile hydrogen, rather than trapped hydrogen.

Hydrogen-related phenomena in steel are generally categorized as internal hydrogen embrittlement (IHE) or hydrogen environment embrittlement (HEE) depending on the sequence of hydrogen dissolution and stress application [26]. In IHE, hydrogen dissolution and stress application occur sequentially, while in HEE, both processes happen concurrently [7].

Despite extensive research, the precise mechanisms by which hydrogen affects the mechanical properties of metals are not fully understood [34] [35]. Several theories have been proposed to explain hydrogen-assisted cracking [36]. One of the oldest is the pressure theory, which attributes cracking to the recombination of atomic hydrogen in metal defects such as voids. The pressure generated by molecular hydrogen inside the voids accelerates void growth and the crack propagation. For hydride-forming materials like niobium, vanadium, and zirconium, hydrogen-assisted cracking occurs through the repeated formation and fracture of brittle hydrides at crack tips [36].

Another theory, known as the Surface Energy theory, suggests that hydrogen absorption reduces the energy required to create new surfaces during crack propagation, thus lowering the work of fracture.

The Hydrogen Enhanced Decohesion (HEDE) mechanism, also called Hydrogen Induced Decohesion (HID), theorizes that hydrogen accumulates at crack tips, reducing the cohesive energy of the metal

lattice and resulting in decreased fracture toughness [37] [38]. This theory is often used to explain brittle fractures in metals affected by hydrogen embrittlement.

In contrast, ductile fracture induced by hydrogen can be explained by the Hydrogen Enhanced Localized Plasticity (HELP) theory. According to this model, hydrogen redistributes around dislocations, lowering the elastic interaction energy between them. This reduces the shear stress required to move dislocations, leading to material softening [39].

Another model, the Hydrogen Enhanced Strain-Induced Vacancies (HESIV) theory, proposes that hydrogen promotes the formation and agglomeration of vacancies during strain, which facilitates the linking of microvoids and contributes to fracture [40]. Nagumo et al. showed that hydrogen negatively affects both crack initiation and crack growth rate in low-alloyed steels [40].

Srinivasan and Neeraj suggested that failure modes can shift from ductile to quasi-brittle fractures as yield strength increases and/or stress state triaxiality rises. A combination of HELP, HEDE, and HESIV mechanisms might be required to fully explain the embrittlement process [30]. The Adsorption-Induced Dislocation Emission (AIDE) mechanism is also noteworthy, as it combines aspects of HELP and HEDE: hydrogen weakens interatomic bonds (as per HEDE), but crack growth occurs through localized slip (as per HELP) [36].

In hydrogen embrittlement, crack growth is controlled by the rate of hydrogen transport to the crack tip, the applied stress, and the metal's intrinsic susceptibility.

## 5. HYDROGEN EMBRITTLEMENT OF NATURAL GAS PIPELINE STEELS

In the absence of microstructural alterations, pipeline steels are generally immune to hydrogen embrittlement, even under cathodic protection at very low potentials [41] [42]. Hydrogen-induced cracking in pipelines has only been observed in rare cases involving slow plastic deformation, such as in buried pipelines affected by mechanical damage or landslides [43] [44].

However, the presence of hard spots—microstructural anomalies typically caused by manufacturing defects or welding—can make pipeline steels more susceptible to brittle fracture in the presence of hydrogen [45] [46]. Hard spots are characterized by hard, untempered martensitic or bainitic structures, often found in steels with high carbon, sulfur, or manganese content. The critical role of hard spots in hydrogen embrittlement can be attributed to the martensitic structure, which is particularly vulnerable to hydrogen [29] [47] [48].

High-strength steels are more prone to hydrogen embrittlement, even under static loading conditions. The presence of hydrogen recombination poisons, such as $H_2S$ or $NaSO_2$, can enhance hydrogen absorption, making these steels more susceptible to embrittlement, even in weakly acidic environments like rain [49].

The effects of gaseous hydrogen on materials are similar to those observed under cathodic polarization: embrittlement increases with the mechanical strength of the material and is more pronounced in welds and heat-affected zones (HAZ). Ferritic/pearlitic steels, particularly those with banded microstructures,

show greater susceptibility compared to sorbitic microstructures. There is a strong correlation between strain rate and hydrogen embrittlement, with slower strain rates leading to more pronounced effects.

Differences between hydrogen uptake via gaseous hydrogen and electrochemical charging seem to be mainly related to the total amount of hydrogen entering the metal. Gaseous hydrogen absorption is typically much lower than that introduced via cathodic polarization, which is why very high hydrogen pressures are required to observe embrittlement effects at low temperatures.

In pipeline steels, gaseous hydrogen primarily accelerates fatigue crack growth and contributes to subcritical crack growth in the HAZ of welds. Hydrogen embrittlement effects are also evident in slow strain rate tests, which typically show a reduction in total elongation and area reduction percentages [26]. Under dynamic loading conditions, superficial oxides that inhibit hydrogen adsorption can be broken, intensifying embrittlement phenomena.

## 6. HYDROGEN SOLUBILITY AND DIFFUSION IN CAST IRON

Hydrogen can be introduced into cast iron either through gaseous or electrochemical charging, although electrochemical methods are generally considered more effective [50]. Most data on hydrogen solubility and diffusion focus on spheroidal cast iron, with results varying depending on factors such as matrix structure (ferritic or ferritic-pearlitic), graphite spheroid size, and loading conditions. Yoshimoto et al. measured hydrogen concentrations ranging from 7.8 to 65.9 mass ppm in thin (1 mm) chips of nodular cast iron with different graphite nodule sizes. These samples were hydrogen-charged in 20% thiocyanate at 40 °C for 168 hours. They found that hydrogen concentration increases with the diameter of the graphite nodules (Figure 9) [51].

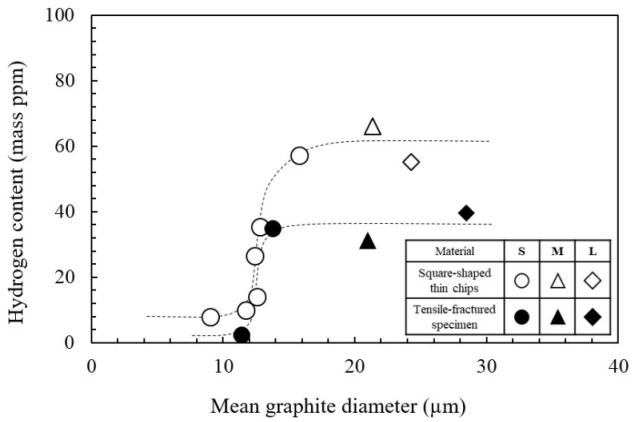


Figure 9. Relationship between hydrogen content of tensile fractured specimens and mean graphite spheroid diameter [51]

The same authors also measured the apparent hydrogen diffusion coefficient by monitoring residual hydrogen content ($C_{H,R}$) as a function of holding time in ambient air following hydrogen charging, $\Delta t$ (Figure 10). After 200 hours, the hydrogen content decreased to the level found in non-charged specimens, indicating that most of the absorbed hydrogen was diffusive. The apparent hydrogen

diffusion coefficient at room temperature was estimated to be $D' = 9.1 \times 10^{-13}$ m$^2$/s, which is lower than the diffusion coefficient in steels, likely due to the presence of graphite nodules in the microstructure [52].

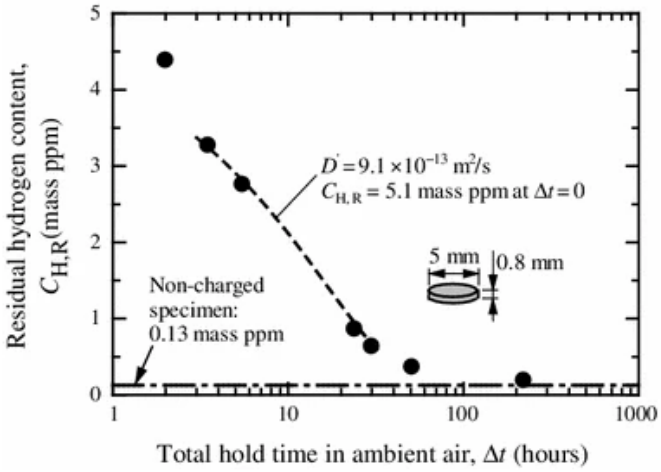


Figure 10. Residual hydrogen content as a function of total hold time in ambient air (Broken line shows the least-square fitting with Demarez et al.'s solution for the hydrogen diffusion from a finite cylinder) [52]

Ogi et al. [53]. used the electrochemical hydrogen permeation method to evaluate hydrogen diffusion and absorption in ferritic spheroidal graphite cast iron. Their results showed that the hydrogen diffusion coefficient of cast iron was lower than that of steel, even when both had the same alloy composition in their ferritic matrices (Figure 11). Their data, however, was significantly higher than the values reported by Matsunaga et al. [54].

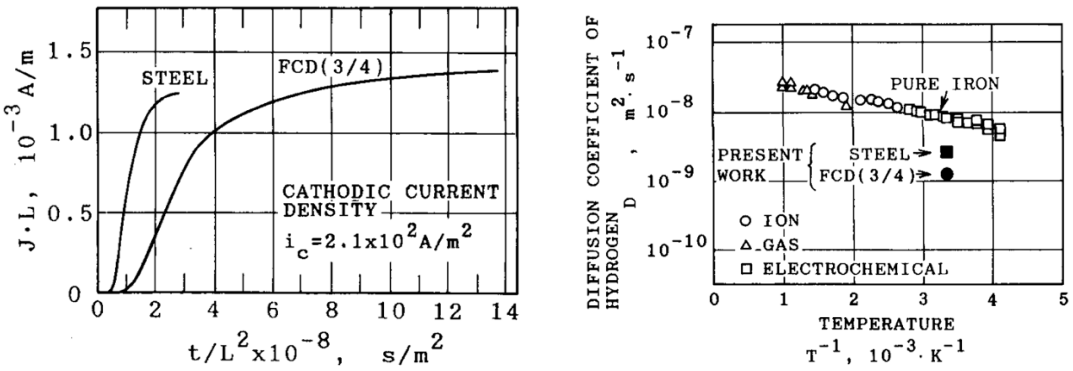


*a)* *b)*

Figure 11. a) Permeation curves of steel and ferritic cast iron (FCD); b) Diffusion coefficient of hydrogen in steel and FCD measured by electrochemical permeation method which are compared with previous data obtained by gas (Δ), ion (○) and electrochemical (□) charging methods [53]

In steady-state conditions, the hydrogen content was higher in ferritic spheroidal cast iron compared to steel (Figure 12). This was attributed to the ability of graphite nodules to store large amounts of hydrogen, both within the graphite itself and at the graphite-matrix interface (Figure 13) [53].

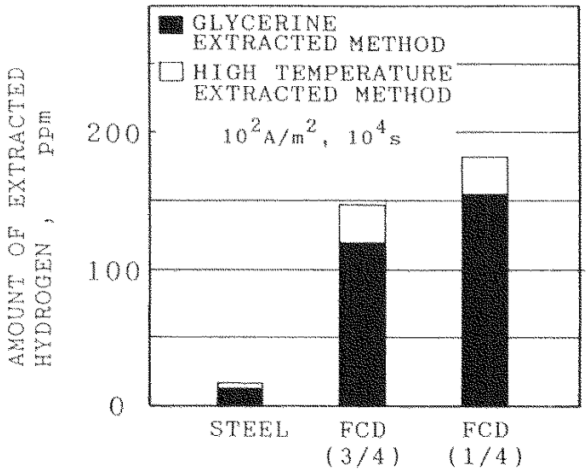


Figure 12. Relation between species of specimens and amount of hydrogen in specimens measured by glycerin extracted method and high temperature extracted method [53]

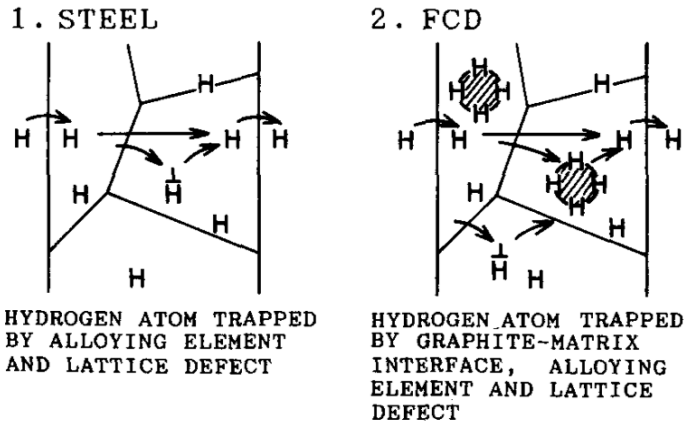


Figure 13. Schematic illustration of behavior of hydrogen in steel and FCD: ⊥ lattice defects and Ø spheroidal graphite [53]

The hydrogen storage ability of graphite was further demonstrated by hydrogen microprint techniques (HMT) used by Matsunaga et al. [52] [54] to visualize hydrogen near the graphite/matrix interface (Figures 14 and 15). These studies showed that spheroidal graphite has a layered crystalline structure with strong covalent bonds between atoms and weak molecular forces between layers, consequently, numerous interlayers within a graphite nodule can serve as a storage site for substantial amount of hydrogen [52].

Takai et al. [55] used Thermal Desorption Spectroscopy (TDS) and Secondary Ion Mass Spectrometry (SIMS) to analyze hydrogen absorption in ferritic spheroidal graphite cast iron. After charging specimens in 20% $NH_4SCN$ at 50 °C for 24 hours, they observed two hydrogen desorption peaks: one at 200-250 °C, corresponding to hydrogen trapped at dislocations and ferrite/cementite ($Fe_3C$) interfaces (21.6 kJ/mol),

and another at 440-460 °C, corresponding to hydrogen strongly trapped within graphite (105.8 kJ/mol) (Figure 16).

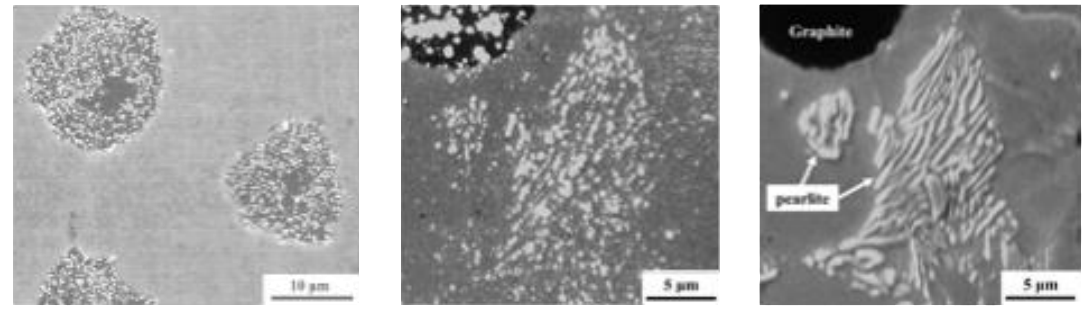


(a) Hydrogen emission from graphite (b) Hydrogen emission from pearlite, HMT image (*left*); Etched microstructure at the same area (*right*)

Figure 14. Microprinting images of hydrogen trapped in the correspondence of graphite and pearlite [54]

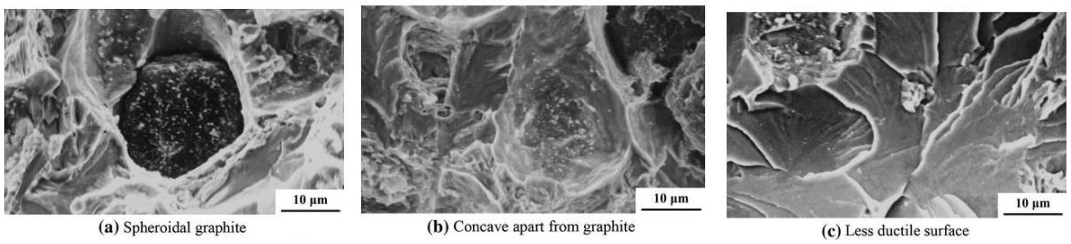


(a) Spheroidal graphite (b) Concave apart from graphite (c) Less ductile surface

Figure 15. HMT images on the fracture surfaces of the hydrogen-charged specimen after SSR tests with cross head speed 1.0 mm/min [52]

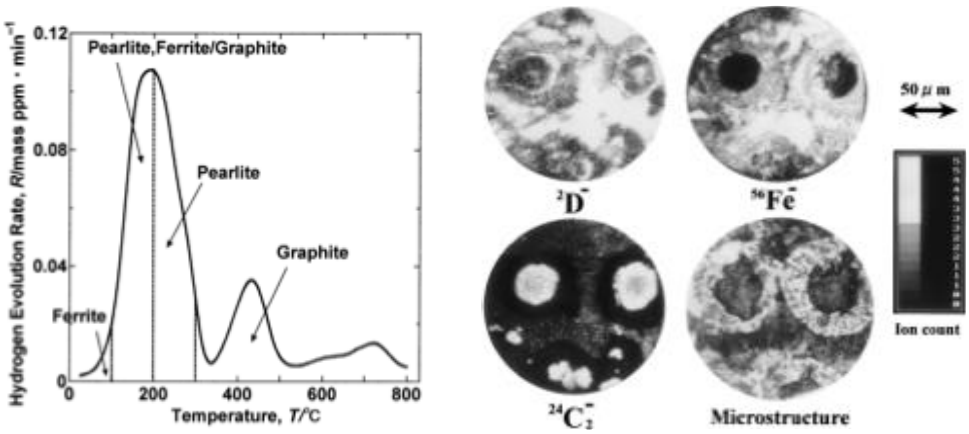


*a)* *b)*

Figure 16. a) Schematic diagram of desorption sites corresponding to the desorption profile in spheroidal graphite cast iron; b) Secondary ion images of $^{2}D^{-}$, $^{56}Fe^{-}$ and $^{24}C_2^{-}$ obtained by SIMS and optical microstructure of spheroidal graphite cast iron. These images are measured immediately after occluding hydrogen and deuterium [53]

Forsström et al. obtained similar TDS results, although their charging conditions differed. They electrochemically charged spheroidal cast iron in a de-aerated 1 N $H_2SO_4$ solution with 10 mg/L thiourea,

at an applied potential of −950 mV vs. $Hg/Hg_2SO_4$. After constant strain rate and constant load tests (CLT), they found a shift in desorption peaks and a significant increase in total hydrogen content. Hydrogen concentrations varied from 8 ppm after 1 hour of charging to 10-20 ppm after constant strain rate tests. After constant load tests, the hydrogen concentration increased further, with values from 111.2 wt. ppm after 11.2 h in CLT, up to 279.7 wt. ppm after 22.4 h [62].

Wu et al. [50] reported that nodular cast iron electrochemically charged with hydrogen in a $Na_2SO_4$ and $As_2O_3$ solution could reach hydrogen concentrations higher than 50 wt. ppm near the surface, although concentrations decreased rapidly with increasing depth (for comparison, as-received bulk cast iron is at 1.7 wt. ppm). They proposed a relationship between hydrogen concentration *H* (in wt. ppm), depth *D* (in mm), and constants α and β that depend on charging time (Table 1):

$$H = \alpha \cdot D^{\beta} \quad (17)$$

Table 1. Values of α and β as a function of the charging time [50]

| Charging time | α | β |
|---|---|---|
| 8 hours | 7.21 | -0.824 |
| 16 hours | 6.092 | -0.533 |
| 48 hours | 12.06 | -0.303 |
| 504 hours | 22.68 | -0.294 |

## 7. HYDROGEN EMBRITTLEMENT OF CAST IRON

Cast iron is classified by the Guide to Safety of Hydrogen and Hydrogen Systems (AIAA G-095–2004) [56] as "Not permitted" for hydrogen gas service, based on NASA's hydrogen embrittlement research [57] and associated safety guidelines [58]. Turola et al. [59] found no significant hydrogen embrittlement in cast irons with different microstructures after exposing the material to a 20% $H_2$ and 80% $N_2$ atmosphere at 150 bar and 300°C for 7 days, or after electrochemical charging at 16 mA/cm$^2$ for 24 hours. The authors concluded that graphite nodules in cast iron could accommodate diffused hydrogen, thereby delaying embrittlement. The amount and morphology of graphite, along with the presence of alloying elements and phases, play a key role in this resistance. Similarly, Birkitt et al. [60] found no hydrogen effect on the mechanical properties of cast iron after tensile testing specimens exposed to 100% $CH_4$ or a blend of 80% $CH_4$ and 20% $H_2$ at 2 bar and 20°C for 6 weeks. Ferrarese et al. [61] also confirmed increased hydrogen content in cast iron alloys after exposure to 20% $H_2$ and 80% $N_2$ at 300°C and 150 bar for 7 days. However, mechanical tests conducted immediately after exposure showed no significant impact of hydrogen on the alloys.

Conversely, ductility loss due to hydrogen was observed during slow strain rate tests on electrochemically charged ductile cast iron. The reduction in the area ratio decreased with increasing graphite diameter, corresponding to increased hydrogen content (Table 2 and Figures 17-18) [51].

Table 2. Mean graphite diameter, RRA and Hydrogen content for the different ductile cast iron [51]

| Material | Mean graphite diameter (μm) | RRA | Hydrogen content (mass ppm) |
|---|---|---|---|
| $S_L$ | 11.4 | 0.77 | 2.3 |
| $S_U$ | 13.8 | 0.38 | 34.8 |
| M | 21.0 | 0.48 | 31.3 |
| L | 28.5 | 0.43 | 39.7 |

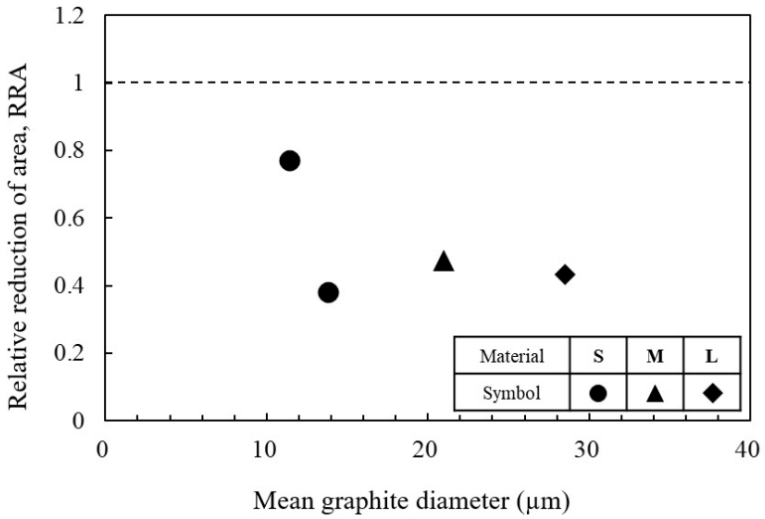


Figure 17. relationship between RRA and mean graphite diameter [51]

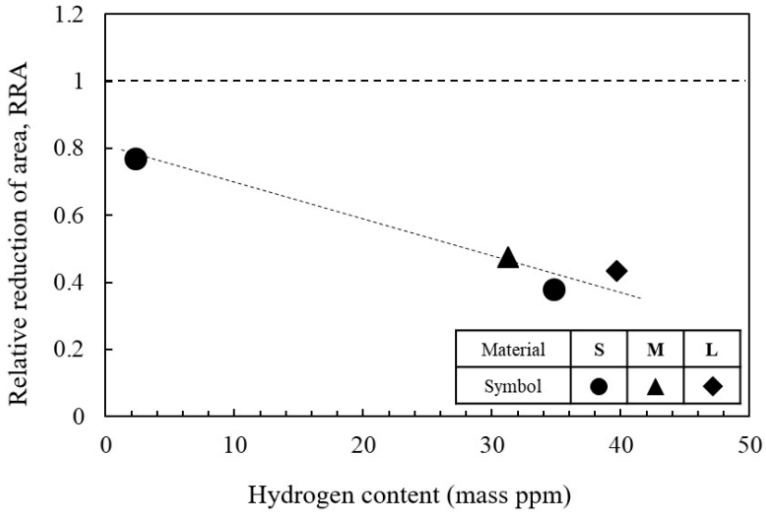


Figure 18. relationship between RRA and hydrogen content [51]

The hydrogen-charged specimens showed a significant reduction in both percentage elongation at fracture and reduction of area as the crosshead speed (CHS) decreased (Figure 19). The fracture surface remained macroscopically perpendicular to the loading direction, regardless of the hydrogen-charging

or CHS (Figure 20). The fracture morphology became notably less ductile in the hydrogen-charged specimens as the CHS decreased (Figure 21). Metallographic sections of the specimens (Figure 22) revealed that fracture growth occurred through interconnecting cracks between adjacent graphite nodules in the hydrogen-charged specimens, particularly at lower CHS [52].

The cracking mechanism is illustrated schematically in Figure 23: hydrogen accumulates in the graphite and at the graphite/matrix interface, inhibiting the formation of ductile dimples and promoting cracking. During the fracture process, hydrogen is continuously emitted from the graphite, and this delayed hydrogen release contributes to the time-dependent degradation of the material [52].

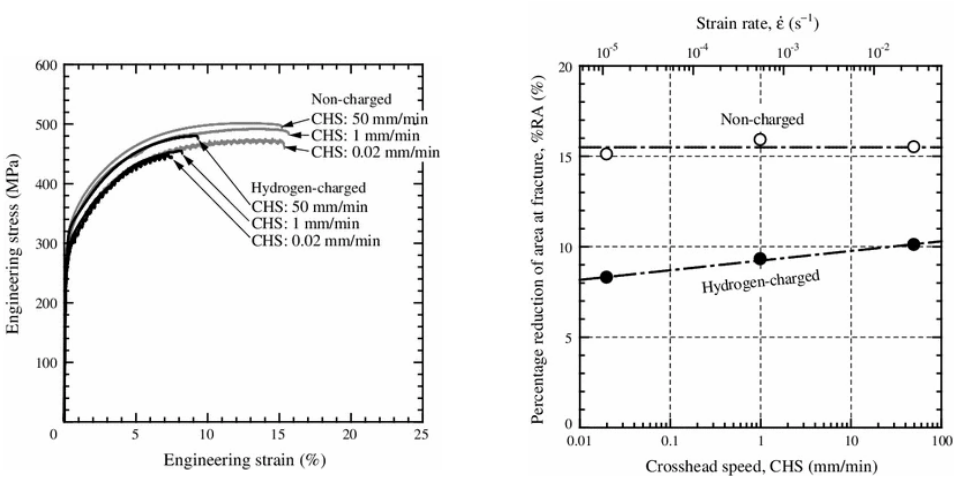


[62]

a) b)

Figure 19. a) Engineering stress–strain curves (CHS: crosshead speed); b) Relationship between the percentage reduction of area and the CHS [52]

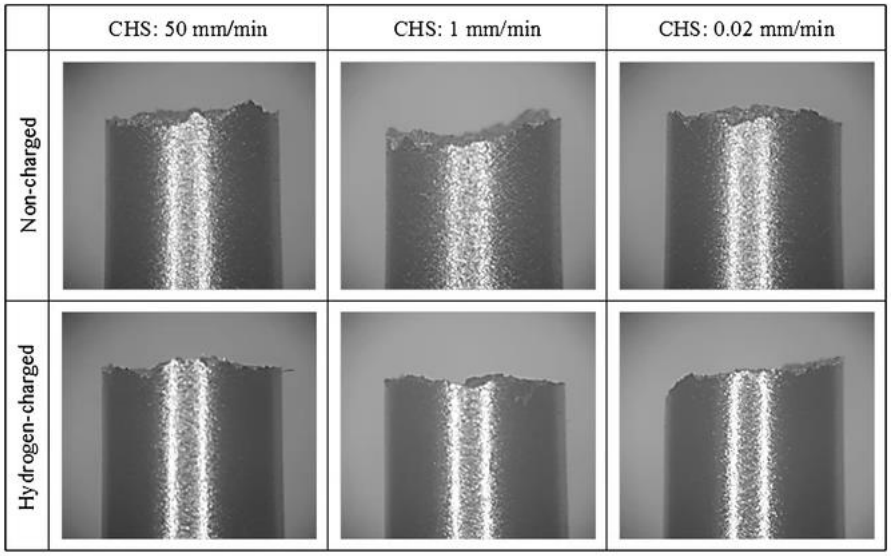


Figure 20. Macroscopic observation of fractured specimens (CHS: crosshead speed) [52]

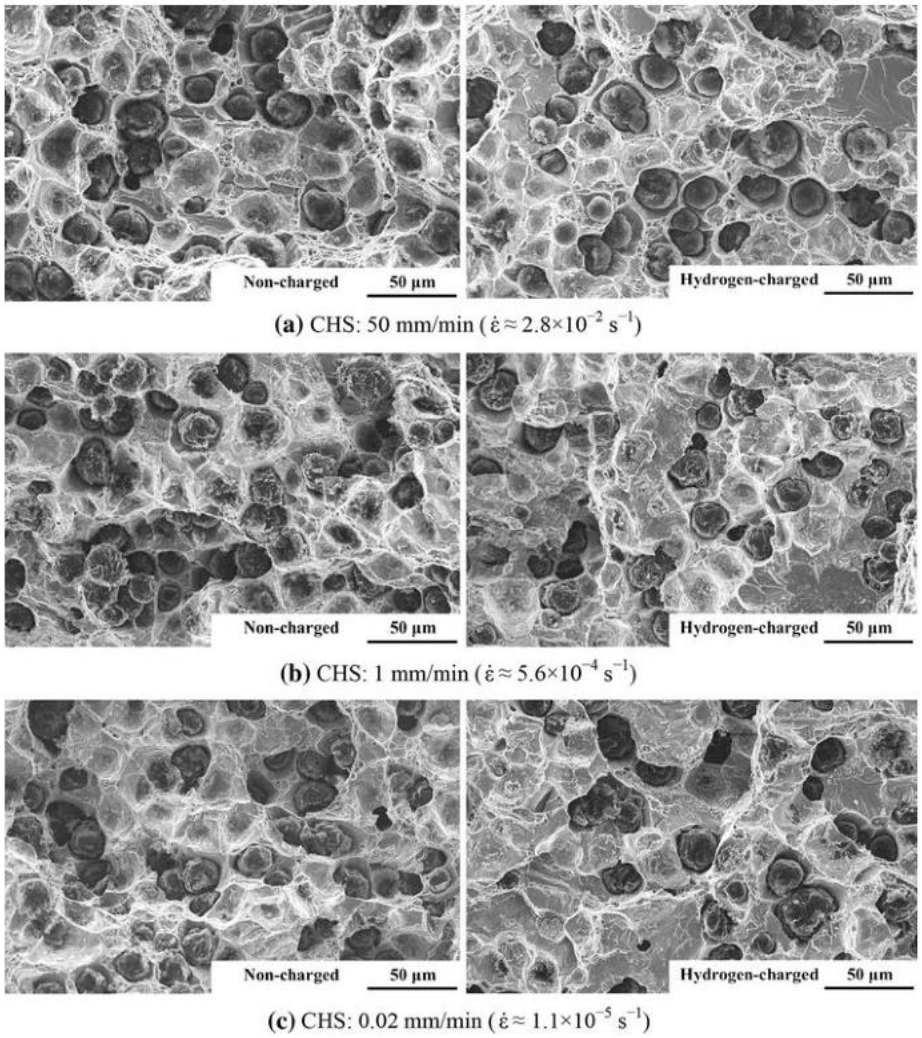


Figure 21. SEM micrographs at the central part of the fracture surfaces (CHS: crosshead speed) [52]

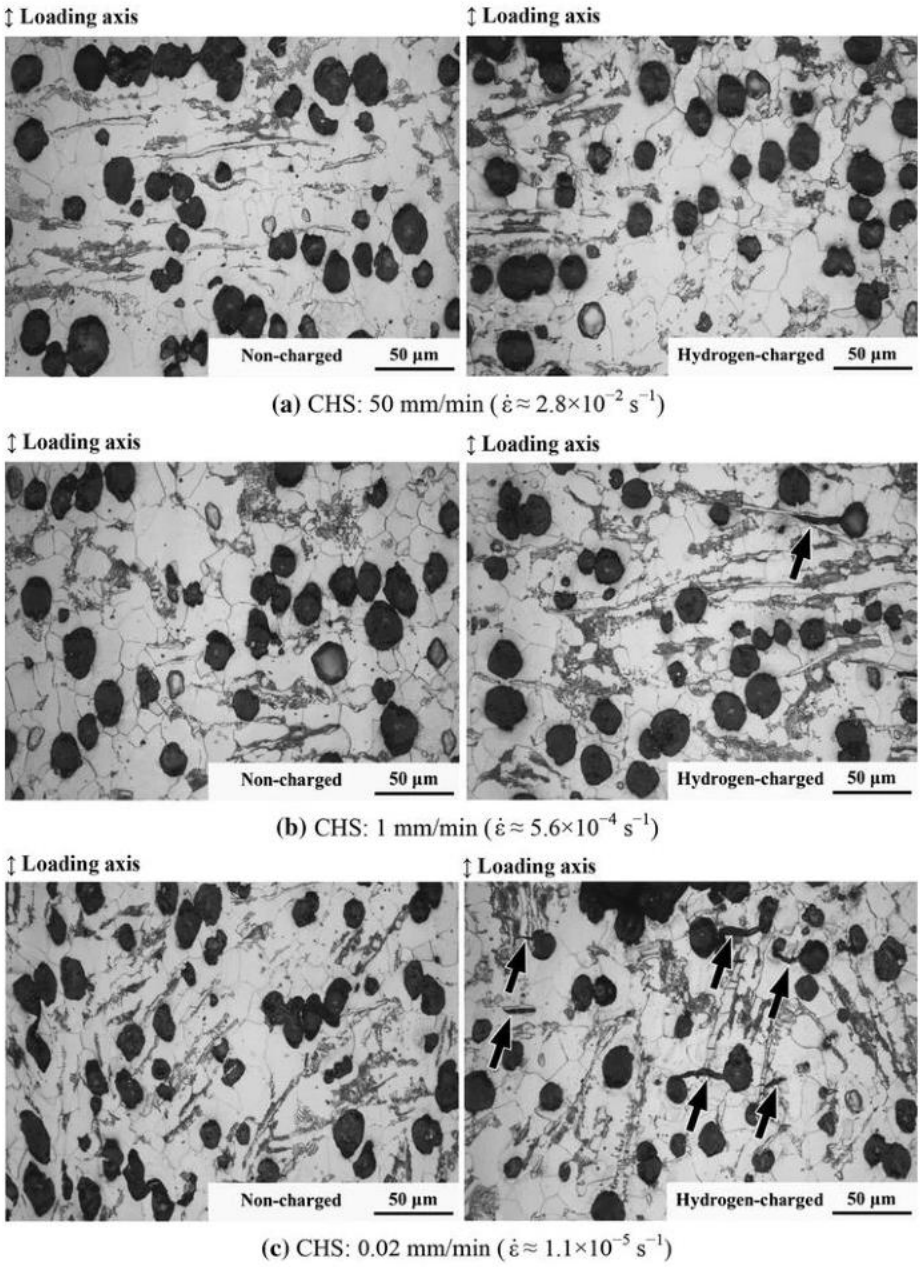


Figure 22. Fracture morphology on the etched longitudinal sections just beneath the fracture surfaces (Arrows indicate interconnecting cracks. CHS: crosshead speed) [52]

These findings are consistent with those reported in two other studies by the same authors, who performed constant strain rate and constant load tests on nodular cast iron while simultaneously applying hydrogen electrolytic charging in a 0.1N $H_2SO_4$ solution with 10 mg/L thiourea. They observed the initiation of small cracks at the interfaces between graphite nodules and the ferrite matrix during the early stages of hydrogen uptake. This confirmed the high hydrogen content at the graphite nodules and the graphite/ferrite matrix interface, which acts as a continuous source of hydrogen during crack growth [62] [63].

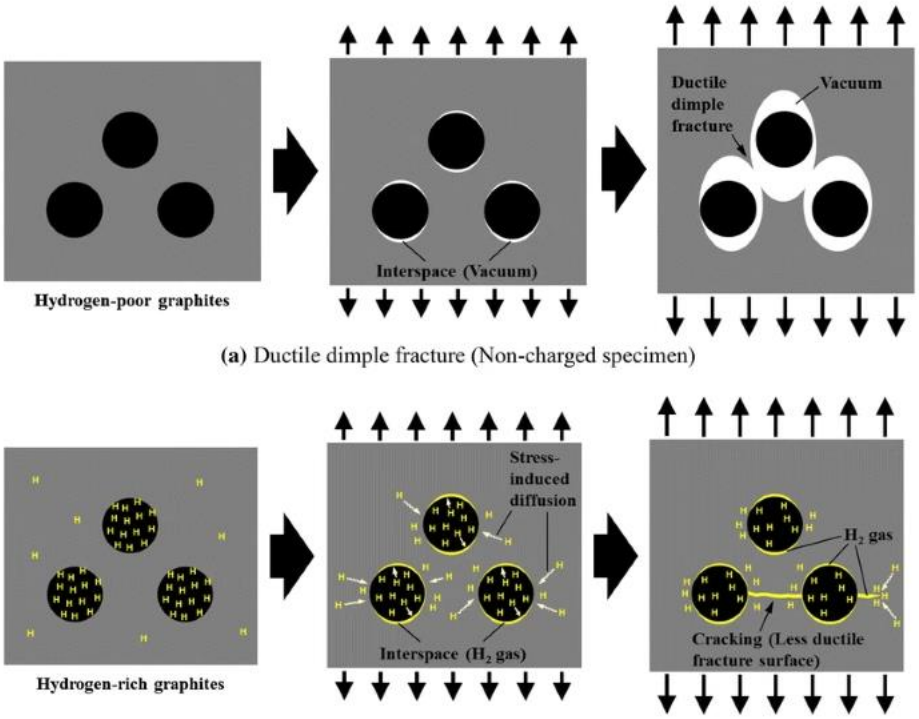


Figure 23. schematic representation of typical fracture processes in the non-charged and the hydrogen-charged specimens [52]

The fatigue crack growth (FCG) rate in pure hydrogen is significantly higher than in air, with the effect becoming more pronounced as the loading frequency decreases. At room temperature (RT), the FCG rate in hydrogen is up to 10 times higher than in air. However, this detrimental effect of hydrogen is mitigated when the temperature is increased to 90°C and 150°C [52]. The reduction in hydrogen trap-site occupancy at dislocation cores is thought to be the reason for this improvement. The presence of a 0.1 vol.% oxygen impurity also inhibits hydrogen uptake in the crack-tip zone, reducing the hydrogen-induced acceleration of FCG. This inhibitory effect of oxygen becomes less significant at higher temperatures [58].

## 8. HYDROGEN SOLUBILITY AND DIFFUSION IN COPPER AND ITS ALLOYS

Hydrogen can be absorbed into copper in atomic form via thermal charging, cathodic charging, or electroless copper plating [64].

Thermal charging typically occurs during metallurgical practices, where copper is annealed in hydrogen gas to reduce defects, increase grain size, or remove oxides. Although copper can absorb significant amounts of hydrogen at elevated temperatures, it tends to spontaneously form gas bubbles due to hydrogen's low solubility at room temperature.

Electrochemical methods are often used to saturate copper with hydrogen at low temperatures, particularly when using recombination inhibitors such as $As_2O_3$. As in thermal charging, maintaining hydrogen supersaturation is difficult, leading to the formation of high-pressure hydrogen bubbles ($H_2$) in

voids, which can also act as traps for diffusing hydrogen, giving erroneously low diffusivity values. These bubbles can also cause structural defects, such as dislocations, as shown in Figure 24 [64].

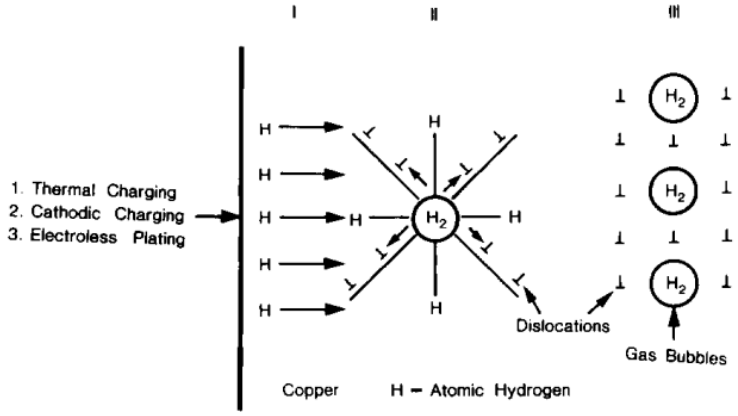


Figure 24. Schematic illustration showing how atomic hydrogen introduced by cathodic or thermal charging and electroless plating produce copper with high density of gas bubbled and dislocations [64]

Hydrogen damage in copper can also occur due to the presence of oxygen. Since oxygen has very low solubility in copper, it forms $Cu_2O$ at interdendritic and grain boundaries during copper's metallurgical processing. Hydrogen, when present at temperatures above 400°C, reacts with oxygen to form steam bubbles within the grains or along grain boundaries, which weakens the material. This phenomenon, known as "hydrogen sickness," can be controlled by minimizing oxygen levels [65].

The solubility of atomic hydrogen in copper decreases significantly with temperature. Nakahara et al. derived the following relationship between hydrogen solubility θ and temperature T (in Kelvin) [64]:

$$(18) \quad ln\theta = \frac{6.62 \cdot 10^3}{T} - 4.48$$

Equilibrium hydrogen solubility in copper increases with rising hydrogen gas pressure (expressed as the square root of pressure), although at room temperature, solubility remains very low even under extremely high pressures (e.g., 8 x $10^{-5}$ ppm at 700 atm) [66].

Horinouchi et al. measured hydrogen permeation through copper using tritium tracer techniques. They calculated the permeation coefficient Φ using the following equation [66]:

$$(19) \quad \Phi = \alpha \cdot \frac{d}{\sqrt[2]{P}}$$

Where α is the amount of hydrogen permeating through the membrane per unit time and area, *d* is the membrane thickness, and *P* is the hydrogen pressure. The permeation coefficient is temperature-dependent, following an Arrhenius relationship in the range of 300-1000 K (figure 25):

$$(20) \quad \Phi = (2.8 \pm 0.4) \times 10^{-6} e^{\left(\frac{-85 \pm 2(kJ/mol)}{RT}\right)} \quad mol \cdot m^{-1} \cdot s^{-1} \cdot Pa^{-\frac{1}{2}}$$

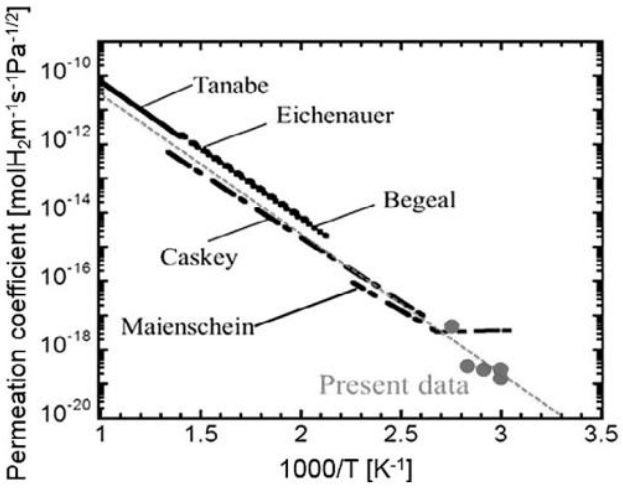


Figure 25. Temperature dependence of permeation coefficient of hydrogen in Cu literature data and results of [66]

The temperature dependence of the apparent diffusion coefficient, as reported by Horinouchi et al., is shown in Figure 26. The deviation observed between the extrapolated data from elevated temperatures (above 473 K) to near room temperature is attributed to the hindering effect of surface oxides. These oxides are gradually removed during hydrogen permeation, preventing them from affecting the steady-state permeation process [66].

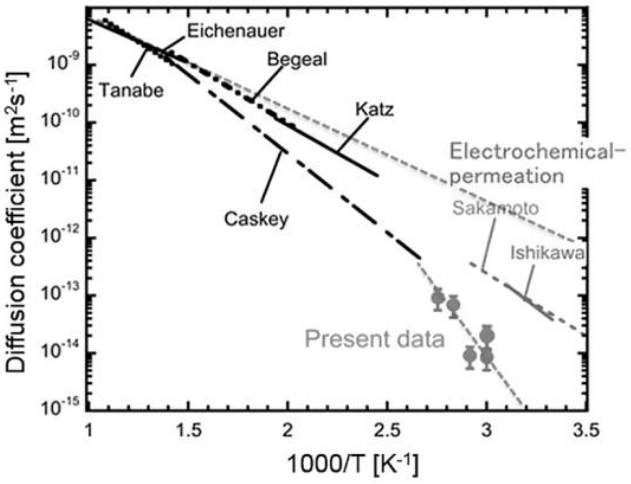


Figure 26. Temperature dependence of diffusion coefficient of hydrogen in Cu [66]

Yamabe et al. found similar values for hydrogen solubility and diffusivity in a high-strength copper-beryllium alloy. The alloy was heat-treated through annealing, straining, and aging at 588 K for 2 hours, followed by hydrogen gas charging at 100 MPa and temperatures of 543 K or 573 K, for durations ranging from 300 to 500 hours (Figure 27) [67].

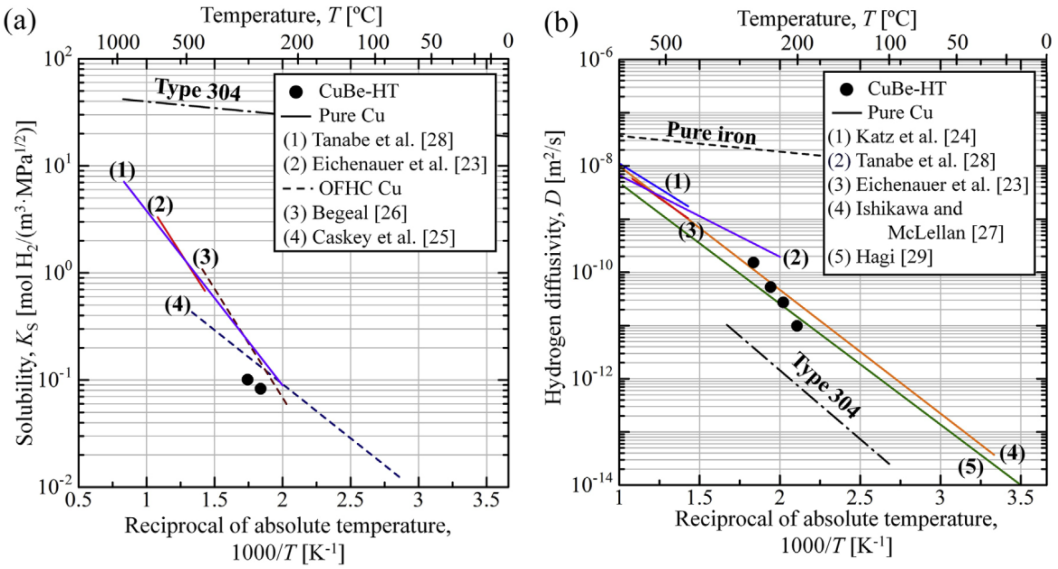


Figure 27. Arrhenius plot of: (a) hydrogen solubility and (b) hydrogen diffusivity

## 9. HYDROGEN DAMAGE OF COPPER

At room temperature, the equilibrium solubility of hydrogen in copper is very low, and atomic hydrogen alone does not significantly affect copper's properties. Hydrogen introduced through electrochemical charging remains concentrated near the surface, penetrating no deeper than 50 µm [68]. However, hydrogen can form gas bubbles near the surface, which might increase microhardness, as observed by Al-Marahleh and El-Amoush [69]. Microhardness increases with both the applied cathodic current density and the duration of hydrogen charging.

NASA's technical report on hydrogen embrittlement found that hydrogen has a negligible effect on copper and its alloys at room temperature and under hydrogen pressures up to 68.9 MPa [57]. Similarly, Birkitt et al. found no hydrogen-induced effects on copper or soldered copper in tensile tests at $2.53 \cdot 10^{-4}$ $s^{-1}$ conducted after 6 weeks of exposure to a gaseous environment at 2 bar and 20°C (in atmospheres of 100% $CH_4$ or 80% $CH_4$ and 20% $H_2$) [60].

In the Sandia Report SAND2012-7321 San Marchi and Somerday reported the data present in Fidelle et al. that didn't show any hydrogen effect on copper in disk rupture tests [70].

However, minor hydrogen effects were observed in oxygen-free copper during slow strain rate (SSR) and constant load tests, performed under continuous electrochemical hydrogen charging. Precharging was done for 3 hours in a 1N $H_2SO_4$ solution containing $NaAsO_2$ at −1.1 V vs. $Hg/H_2SO_4$, at both 20°C and 50°C. SSR tests, carried out at a strain rate of $10^{-5}$ $s^{-1}$, showed a 10% reduction in fracture elongation at both temperatures, as well as a slight decrease in tensile strength at 50°C. Shallow intergranular cracks, formed by hydrogen-filled voids along grain boundaries, were observed only on the fracture surfaces close to the penetration sites of hydrogen while the overall fracture surface appears fully ductile (Figure 28) [71].

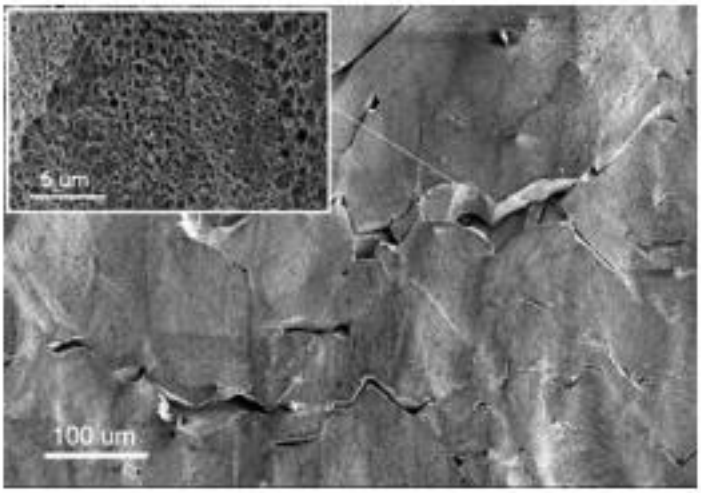


Figure 28. Micrograph of the surface cracks forming on the tensile specimen of the oxygen free phosphorous doped copper in SSR tests with continuous hydrogen charging at 50 °C and a strain rate of $10^{-5}$ $s^{-1}$. The inset shows the dimpled facets formed on the intergranular fracture surfaces [71]

In constant load tests under similar charging conditions of SSR test, hydrogen enhanced the creep rate of copper. The effect was more pronounced at lower applied stresses (resulting in lower creep rates). Creep fractures exhibited dimpled intergranular characteristics, originating from hydrogen-filled voids along grain boundaries, particularly on planes of maximum shear stress (Figure 29). The authors suggested that hydrogen damage in copper may occur via the Hydrogen Enhanced Localized Plasticity (HELP) mechanism [71].

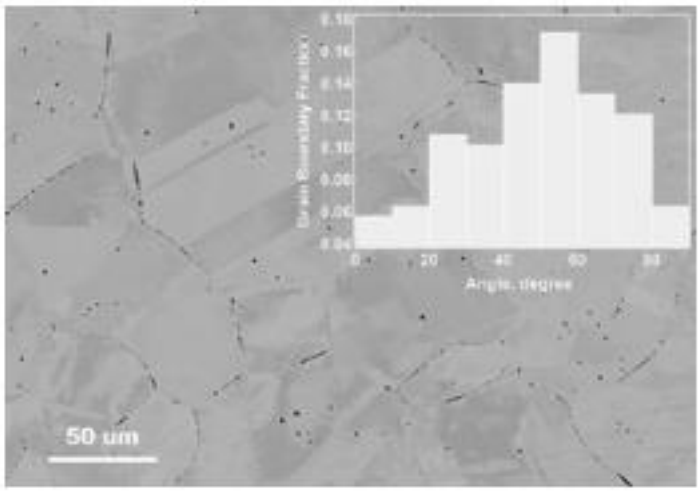


Figure 29. The hydrogen-filled micro voids in the oxygen free phosphorous doped copper tested at an applied stress of 80 MPa under continuous hydrogen charging at 50 °C. The voids form nets along some of the grain boundaries, the orientation distribution of which is shown relative to the applied loading direction (horizontal) in the inset [71]

# 10. HYDROGEN DIFFUSION AND EFFECT ON LEAD

There is limited literature on the interaction between lead and gaseous hydrogen. At high temperatures, hydrogen can react with lead to form hydrides. Birkitt et al. conducted tensile tests on copper specimens soldered with lead-based solder after 6 weeks of exposure to hydrogen-containing gas environments at 2 bar and 20°C. The gas compositions tested were 100% $H_2$, 80% $CH_4$ + 20% $H_2$, 100% $CH_4$. The tests, conducted according to BS EN ISO 6892-1:2016 standards with a strain rate of $2.53 \cdot 10^{-4}$ $s^{-1}$, showed no significant difference between control samples and those exposed to 100% $H_2$ or 80% $CH_4$ + 20% $H_2$. Failures were attributed to bonding defects rather than hydrogen effects [60].

Freiman and Titov studied hydrogen diffusion rates through Armco iron sheets (0.17 mm thick) coated with different metals and cathodically polarized in $H_2SO_4$ with $NaAsO_2$. Thin coatings of Cu, Sn, Pb, or Ni slowed down hydrogen penetration into the iron when $H^+$ discharged on the coating. Nickel coatings (0.1-2.5 µm thick) were particularly effective, whereas lead coatings required a thickness of 10 µm to achieve similar results [72]. The authors concluded that metal coatings can protect against hydrogen penetration by altering hydrogen ion discharge kinetics. Lead, in particular, has a high overpotential for hydrogen evolution [73], but at very high cathodic current densities in alkaline or weakly acid solutions, lead can degrade through the formation of a volatile lead hydride, which later decomposes [74].

## 11. CONCLUSION

In the present document the hydrogen adsorption and absorption into metal are reviewed, focused on the metallic materials identified in D 2.1 of Task 2.1 “Technical report considering the data collection about the non-steel metallic materials used in the natural gas distribution grid”. Cast iron, copper and lead are considered.

Literature date reports no HE effects on cast iron exposed to gaseous hydrogen at room temperature. Cast iron could show HE effects if exposed to gaseous hydrogen at high temperature or cathodically polarized in solution in the presence of hydrogen recombination poisons (like $Na_2AsO_3$ or Thiourea). In this last case, the HE effects are related to size and distribution of graphite nodules and/or pearlite islands. Copper and lead do not show any HE effects at room temperature.

## 12. ACKNOWLEDGEMENTS

The project is supported by the Clean Hydrogen Partnership and its members.

# REFERENCES


[1] R. Gangloff e B. Somerday, Gaseous hydrogen embrittlement of materials in energy technologies. Volume 1 The problem, its characterisation and effects on particular alloy classes, Cambridge (UK) : Woodhead Publishing Limited, 2012.

[2] A. A. Pisarev, «Hydrogen adsorption on the surface of metals,» in *Gaseous hydrogen embrittlement of materials for energy techologies* .

[3] K. Christmann, «Hydrogen Adsorption on metal surfaces,» in *Atomistics of Fracture*, New York , Plenum Press, 1983, pp. 363-389.

[4] A. Campari, F. Ustolin, A. Alvaro e N. Paltrinieri, «A review on hydrogen embrittlement and risk-based inspection of hydrogen technologies,» *International Journal of Hydrogen Energy,* vol. 48, n. 90, pp. 35316-35346, 2023.

[5] S. Sarfaraz, M. Yar, R. Hussain e K. Ayub, «Adsorption and dissociation of $H_2$ molecule over first-row transition metal doped C24 nanocage as remarkable SACs: A comparative study,,» *International Journal of Hydrogen Energy,* vol. 48, n. 54, pp. 20633-20645, 2023.

[6] D. Aireddy e K. Ding, «Heterolytic Dissociation of H2 in Heterogeneous Catalysis,» *ACS Catalysis,* vol. 12, n. 8, pp. 4707-4723, 2022.

[7] A. Staykov, J. Yamabe e B. Somerday, «Effect of hydrogen gas impurities on the hydrogen dissociation on iron surface,» *International Journal of Quantum Chemistry,* vol. 114, n. 10, pp. 626-635, 2014.

[8] V. Gadgeel e D. Johnson, «Gas-Phase Hydrogen Permeation and Diffusion in Carbon Steels as a Function of Carbon Content from 500 to 900 K,» *Journal of Materials for Energy Systems,* vol. 2, pp. 32-40, 1979.

[9] M. Röthig, J. Hoschke, C. Tapia, J. Venezuela e A. Atrens, «A review of gas phase inhibition of gaseous hydrogen embrittlement in pipeline steels,» *International Journal of Hydrogen Energy,* vol. 60, pp. 1239-1265, 2024.

[10] H. Wipf, «Solubility and Diffusion of Hydrogen in Pure Metals and Alloys,» *Physica Scripta,* n. T94, pp. 43-51, 2001.

[11] T. Michler, F. Schweizer e K. Wackermann, «Review on the Influence of Temperature upon Hydrogen Effects in Structural Alloys,» *Metals ,* vol. 11, n. 423, p. https:// doi.org/10.3390/met11030423, 2021.

[12] C. Marchi, B. Somerday e S. Robinson, «Permeability, solubility and diffusivity of hydrogen isotopes in stainless steels at high gas pressures,» *Int. J. Hydrogen Energy ,* vol. 32, p. 100–116, 2007.

[13] R. Oriani, «The diffusion and trapping of hydrogen in steel,» *Acta Metallurgica,* vol. 18, n. 1, pp. 147-157, 1970.

[14] E. Fallahmohammadi, F. Bolzoni, G. Fumagalli, G. Re, G. Benassi e L. Lazzari, «Hydrogen diffusion into three metallurgical microstructures of a Ce Mn X65 and low alloy F22 sour service steel pipelines,» *International journal of hydrogen energy ,* vol. 39, pp. 13300-13313, 2014.

[15] J. Lee e S. Lee, «Hydrogen trapping phenomena in metals with B.C.C. and F.C.C. crystals structures by the desorption thermal analysis technique,» *Surface and Coatings Technology,* vol. 28, p. 301–314, 1986.

[16] G. M. Pressouyre e I. M. Bernstein, «Quantitative analysis of hydrogen trapping,» *Metallurgical Transactions A,* vol. 9, n. 11, pp. 1571-1580, 1978.

[17] E. Villalba e A. Atrens, «SCC of commercial steels exposed to high hydrogen fugacity,» *Engineering Failure Analysis,* vol. 15, p. 617–641, 2008.

[18] V. Olden, A. Senumstad Hauge e O. Magne Akselsen, «The Influence of Plastic Strain on the Effective Hydrogen Diffusion Coefficient and Trapping in Base Metal and Weld Simulated Heat Affected Zone of an X70 Pipeline Steel,» in *Proceedings of the Twenty-second (2012) International Offshore and Polar Engineering Conference*, 2012.

[19] F. Huang, L. Liu, Z. Deng, J. Cheng e Z. Lu, «Effect of microstructure and inclusions on hydrogen induced cracking susceptibility and hydrogen trapping efficiency of X120 pipeline steel,» *Materials Science and Engineering A,* vol. 527, p. 6997–7001, 2010.

[20] H. Xue e Y. Cheng , «Characterization of inclusions of X80 pipeline steel and its correlation with hydrogen-induced cracking,» *Corrosion Science,* vol. 53, p. 1201–1208, 2011.

[21] S. Lee e J. Lee, «The effect of the interface character of TiC particles on hydrogen trapping in steel,» *Acta Metallurgica,* vol. 35, n. 11, pp. 2695-2700, 1987.

[22] M. Stevens e I. Bernstein, «Microstructural trapping effects on hydrogen induced cracking of a microalloyed steel,» *Metallurgical Transaction A,* vol. 20A, p. 909–919, 1989.

[23] R. Valentini, A. Solina, S. Matera e P. De Gregorio, «Influence of titanium and carbon contents on the hydrogen trapping of microalloyed steels,» *Metallurgical and Materials Transactions A,* vol. 27, p. 3773–3780, 1996.

[24] F. Wei e K. Tsuzaki, «Quantitative analysis on hydrogen trapping of TiC particles in steel,» *Metallurgical and Materials Transactions A,* vol. 37, p. 331–353, 2006.

[25] A. Haq, K. Muzaka, D. Dunne, A. Calka e E. Pereloma, «Effect of microstructure and composition on hydrogen permeation in X70 pipeline steels,» *International Journal of Hydrogen Energy,,* vol. 38, n. 5, pp. 2544-2556, 2013.

[26] C. San Marchi e B. Somerday, «Technical reference on hydrogen compatibility of materials,» Livermore CA , 2012.

[27] V. Gadgeel e D. Johnson, «Gas-Phase Hydrogen Permeation and Diffusion in Carbon Steels as a Function of Carbon Content from 500 to 900 K,» *Journal of Materials for Energy Systems,* vol. 1, pp. 32-40, 1979.

[28] Z. Feng, L. Anovitz, P. Kironko, A. Duncan, T. Adams e P. Sofronis, «https://www.energy.gov/sites/prod/files/2014/03/f10/pipeline_group_feng_ms.pdf,» [Online].

[29] J. P. Hirth, «Effects of Hydrogen on the Properties of Iron and Steel,» *METALLURGICAL TRANSACTIONS A,* vol. 11A, pp. 861-890, 1980.

[30] R. Srinivasan e T. Neeraj, «Hydrogen Embrittlement of Ferritic Steels: Deformation and Failure Mechanisms and Challenges in the Oil and Gas Industry,» *JOM,* vol. 66, n. 8, pp. 1377-1382, 2014.

[31] . W. Johnson, «On some remarkable changes produced in iron and steel by the action of hydrogen acids,» *Proceedings of the Royal Society of London,* vol. 23A, pp. 168-179, 1875.

[32] E. Wallaert, T. Depover, B. Pieters, . M. A. Arafin e K. Verbeken, «TDS Evaluation of the Hydrogen Trapping Capacity of NbC Precipitates,» in *International Hydrogen Conference (IHC 2012): Hydrogen-Materials Interactions*, 2014, p. Chapter 62.

[33] A. Zielinski e P. Domzalicki, «Hydrogen degradation of high-strength low-alloyed steels,» *Journal of Materials Processing Technology,* vol. 133, n. 1-2, pp. 230-235, 2003.

[34] C. Beachem, «A New Model for Hydrogen-AssistedCracking (Hydrogen Embrittlement),» *Metallurgical Transactions,* vol. 3, pp. 437-451, 1972.

[35] M. Bernstein e A. Thompson, «Effect of Metallurgical Variables on Environmental Fracture,» *International Metal Review,* vol. 21, pp. 269-87, 1976.

[36] S. Lynch, «Mechanisms of Hydrogen Assisted Cracking - A review,» in *Hydrogen effects on Materials Behavior and Corrosion Deformation Interactions*, vol. 1, TMS (The Mineals, Metals and materials Society), 2003, pp. 449-466.

[37] A. R. Troiano, «The role of hydrogen and other interstitials in the mechanical behaviour of metals.,» in *Trans. ASM 52*, 1960, pp. 54-80.

[38] R. Oriani, «Mechanicistic Theory of Hydrogen Embrittlemnt of Steels,» *Berichte Der Bunsen-Gesellschaft Fur Physikalische Chemie,* vol. 76, n. 8, pp. 848-857, 1972.

[39] C. Ayas, V. Deshpande e N. Fleck, «A fracture criterion for the notch strength of high strength steels in the presence of hydrogen,» *Journal of the Mechanics and Physics of Solids,* vol. 63, pp. 80-93, 2014.

[40] M. Nagumo, «Hydrogen related failure of steels – a new aspect,» *Materials Science and Technology,* vol. 20, n. 8, pp. 940-950, 2004.

[41] M. Cabrini e S. Lorenzi, «Pipeline Steels: Hydrogen Diffusion and Environmentally- Assisted Cracking,» in *Encyclopedia of Iron, Steel, and Their Alloys*, Boca Raton , CRC press, 2016, pp. 2547-2559.

[42] M. Cabrini, S. Lorenzi, S. Pellegrini e T. Pastore, «Environmentally assisted cracking and hydrogen diffusion in traditional and high-strength pipeline steels,» *Corrosion Reviews,* vol. 33, n. 6, pp. 529-54, 2015.

[43] A. Punter, A. T. Fikkers e G. Vanstaen, «Hydrogen- Induced Stress Corrosion Cracking on a Pipeline,» *Materials Performance,* vol. 31, pp. 24-28, 1992.

[44] M. Cabrini , V. Pistone, E. Sinigaglia e M. Tarenzi, «Unique Hsc Scenario Leads To Gas Line Failure,» *Oil & Gas Journal,,* vol. 6, p. 61.65, 2000.

[45] R. Fessler, T. Groeneveld e A. Elsea, «Stress-Corrosion and Hydrogen-Stress Cracking in Buried Pipelines,» in *Stress Corrosion Cracking and Hydrogen Embrittlement of Iron Base Alloys, International Corrosion Conference Series,*, Huston, TX: NACE, 1977.

[46] C. Carter e M. Hyatt, «Review of Stress Corrosion Cracking in Low Alloy Steels with Yield Strength Below 150 ksi,» in *Stress Corrosion Cracking and Hydrogen Embrittlement of Iron Base Alloys*, Houston, NACE, 1977, pp. 524-600.

[47] J. Kim, Y. Lee, D. Lee, K. Park e C. Lee, «Effect of intergranular ferrite on hydrogen delayed fracture resistance of ultrahigh strength boron-added steel,» *ISIJ (The Iron and Steel Institute of Japan) International,* vol. 47, pp. 913-919, 2007.

[48] J. Ham, B. Kim e S. Lee, «Measurement method of sensitivity for hydrogen embrittlement of high strength bolts,» *Korean Journal of Metals and Materials,* vol. 49, pp. 1-8, 2011.

[49] M. Cabrini, S. Lorenzi, T. Pastore e D. Pesenti Bucella, «Effect of hot mill scale on hydrogen embrittlement of high strength steels for pre-stressed concrete structures,» *Metals,* vol. 8, pp. 1-12, 2018.

[50] R. Wu, J. Ahlström, H. Magnusson, K. Frisk e A. Martinsson, «Charging, degassing and distribution of hydrogen in cast iron,» Swerea KIMAB, Stockholm, 2015.

[51] T. Yoshimoto , T. Matsuo e T. Ikeda, «The effect of graphite size on hydrogen absorption and tensile properties of ferritic ductile cast iron,» *Structural Integrity Procedia,* vol. 14, pp. 18-25, 2019.

[52] H. Matsunaga, T. Usuda, K. Yanase e M. Endo , «Ductility Loss in Ductile Cast Iron with Internal Hydrogen,» *Metallurgical and Materials Transaction A,* vol. 45, p. 1315–1326, 2014.

[53] K. Ogi, H. Hagi, A. Tahara, A. Sawamoto, H. Ikeda e Y. Hayashi , «Behavior of Hydrogen in Ferritic Spheroidal Graphite Cast Iron with Heavy Section,» *The Journal of the Japan Foundrymen's Society,* vol. 64, n. 3, pp. 186-191, 1992.

[54] H. Matsunaga, T. Usuda, K. Yanase e M. Endo, «Ductility loss in Hydrogen-charged Ductile Cast Iron,» in *13th International Conference on Fracture*, Beijing, China, 2013.

[55] K. Takai,, K. Chiba, K. Noguchi e A. Nozue , «Visualization of the hydrogen desorption process from ferrite, pearlite, and graphite by secondary ion mass spectrometry,» *Metallurgical and Materials Transactions A,* vol. 33, p. 2659–2665, 2002.

[56] «Guide to Safety of Hydrogen and Hydrogen Systems,» American Institute of Aeronautics and Astronautics, 2004.

[57] J. Lee e S. Woods, «Hydrogen Embrittlement,» NASA, 2016.

[58] K. Okumura, K. Motoyama e H. Matsunaga, «Fatigue crack-growth properties of ductile cast iron in hydrogen gas with oxygen impurity at various temperatures,» *Engineering Failure Analysis,* vol. 158, pp. 108012,, 2024.

[59] J. Turola, R. Obara, A. Ferrarese e A. Albaneze, «Microstructure of cast iron resistant to hydrogen embrittlement,» SAE Technical Paper, 2023-36-0063, 2024.

[60] K. Birkitt, M. Loo-Morrey, A. Bannister, S. Hawksworth, K. Jeffrey e K. Owen, «Materials aspects associated with the addition of up to 20 mol% hydrogen into an existing natural gas distribution network,» Northern Gas Networks Limited, 2019.

[61] A. Ferrarese, E. Kumoto, R. Marquard, M. Wieser, C. Traxler, U. Lundqvist, D. Mumford e J. Walker, «Resistant Cast Iron for a 50% Efficient Hydrogen Engine,» in *International Engine Congress*, Baden Baden (Germany), 2022.

[62] A. Forsström, Y. Yagodzinskyy e H. Hänninen, «Hydrogen effects on mechanical performance of nodular cast iron,» *Corrosion Review,* vol. 37, n. 5, p. 441–454, 2019.

[63] P. Sahiluoma, Y. Yagodzinskyy, A. Forsström, H. Hänninen e S. Bossuyt, «Hydrogen embrittlement of nodular cast iron,» *Materials and corrosion,* vol. 72, pp. 245-254, 2021.

[64] S. Nakahara e . Y. Okinaka, «The hydrogen effect in copper,» *Materials Science and Engineering,* vol. A 101, p. 227–230, 1988.

[65] G. Caskey , A. Dexter, M. Holzworth, M. Louthan e R. Derrick, «Effect of oxygen on hydrogen transport in copper,» *Corrosion,* vol. 32, p. 370–374, 1976.

[66] H. Horinouchi, M. Shinohara, T. Otsuka, K. Hashizume e T. Tanabe, «Determination of hydrogen diffusion and permeation coefficients in pure copper at near room temperature by means of tritium tracer techniques,» *Journal of Alloys and Compounds,* vol. 580, p. S73–S75, 2013.

[67] J. Yamabe, D. Takagoshi, H. Matsunaga , S. Matsuoka, T. Ishikawa e T. Ichigi, «High-strength copper-based alloy with excellent resistance to hydrogen embrittlement,» *International Journal of Hydrogen Energy,* vol. 41, p. 15089e15094, 2016.

[68] A. Martinsson e R. Sandstrom, «Hydrogen depth profile in phosphorus-doped, oxygen-free copper after cathodic charging,» *Journal of Materials Science,* vol. 47, pp. 6768-6776, 2012.

[69] G. Al-Marahleh e A. El-Amoush, «Effect of Cathodically Charged Hydrogen on the Microhardness of Pure Copper,» *American Journal of Applied Sciences,* vol. 2, n. 2, pp. 526-532,, 2005.

[70] R. Bernardi, R. Broudeur, C. Roux e M. Rapin, «Disk Pressure Testing of Hydrogen Environment Embrittlement,» in *Hydrogen Embrittlement Testing*, ASTM STP 543 American Society for Testing and Materials, 1974, pp. 221-253.

[71] Y. Yagodzinskyy, E. Malitckii, T. Saukkonen e H. Hanninen, «Hydrogen-enhanced creep and cracking of oxygen-free phosphorus-doped copper,» *Scripta materialia,* n. 67, pp. 931-934, 2012.

[72] I. Matsushima e H. Uhlig, «Protection of Steel from Hydrogen Cracking by Thin Metallic Coatings,» *Journal of The Electrochemical Society ,* vol. 114, pp. 555-559, 1966.

[73] Z. Jiang, T. Yu, J. Chen, K. Tan, R. Deng, A. Zhou e S. Yin, «Regulating Competitive Adsorption on Pt Nanoparticles by Introducing Pb to Expedite Hydrogen Production via Ammonia Oxidation,» *ACS Applied Nano Materials,* vol. 6, n. 3, pp. 1889-1897, 2023.

[74] H. Salzberg, «Cathodic Lead Disintegration and Hydride Formation,» *Journal of The Electrochemical Society ,* vol. 100, pp. 146-151, 1953.